

# Proton-proton correlations observed in two-proton decay of $^{19}\text{Mg}$ and $^{16}\text{Ne}$

I. Mukha,<sup>1,2</sup> L. Grigorenko,<sup>3,4</sup> K. Sümmerer,<sup>4</sup> L. Acosta,<sup>5</sup> M. A. G. Alvarez,<sup>1</sup> E. Casarejos,<sup>6</sup> A. Chatillon,<sup>4</sup> D. Cortina-Gil,<sup>6</sup> J. Espino,<sup>1</sup> A. Fomichev,<sup>3</sup> J. E. García-Ramos,<sup>5</sup> H. Geissel,<sup>4</sup> J. Gómez-Camacho,<sup>1</sup> J. Hofmann,<sup>4</sup> O. Kiselev,<sup>4,7</sup> A. Korshennikov,<sup>2</sup> N. Kurz,<sup>4</sup> Yu. Litvinov,<sup>4</sup> I. Martel,<sup>5</sup> C. Nociforo,<sup>4</sup> W. Ott,<sup>4</sup> M. Pfützner,<sup>8</sup> C. Rodríguez-Tajes,<sup>6</sup> E. Roeckl,<sup>4</sup> M. Stanoiu,<sup>4,9</sup> H. Weick,<sup>4</sup> and P. J. Woods<sup>10</sup>

<sup>1</sup>Universidad de Sevilla, ES-41012 Seville, Spain

<sup>2</sup>RRC “Kurchatov Institute”, RU-123184 Moscow, Russia

<sup>3</sup>Joint Institute for Nuclear Research, RU-141980 Dubna, Russia

<sup>4</sup>Gesellschaft für Schwerionenforschung, D-64291 Darmstadt, Germany

<sup>5</sup>Universidad de Huelva, ES-21071 Huelva, Spain

<sup>6</sup>Universidade de Santiago de Compostela, ES-15782 Santiago de Compostela, Spain

<sup>7</sup>Johannes Gutenberg Universität, D-55099 Mainz, Germany

<sup>8</sup>IEP, Warsaw University, PL-00681 Warszawa, Poland

<sup>9</sup>IFIN-HH, P. O. BOX MG-6, Bucharest, Romania

<sup>10</sup>University of Edinburgh, EH1 1HT Edinburgh, UK

Proton-proton correlations were observed for the two-proton decays of the ground states of  $^{19}\text{Mg}$  and  $^{16}\text{Ne}$ . The trajectories of the respective decay products,  $^{17}\text{Ne}+p+p$  and  $^{14}\text{O}+p+p$ , were measured by using a tracking technique with microstrip detectors. These data were used to reconstruct the angular correlations of fragments projected on planes transverse to the precursor momenta. The measured three-particle correlations reflect a genuine three-body decay mechanism and allowed us to obtain spectroscopic information on the precursors with valence protons in the  $sd$  shell.

PACS numbers: 21.10.-k; 21.45.+v; 23.50.+z

The recently discovered two-proton (2p) radioactivity is a specific type of genuine three-particle nuclear decays. It occurs when a resonance in any pair of fragments is located at higher energies than in the initial three-body ( $p+p+\text{“core”}$ ) nucleus, and thus simultaneous emission of two protons is the only decay channel. Three-body systems have more degrees of freedom in comparison with two-body systems, hence additional observables appear. In the case of 2p emission, the energy spectra of single protons become continuous, and proton-proton ( $p-p$ ) correlations are available, which makes them a prospective probe for nuclear structure or/and the decay mechanism. For example, the first  $p-p$  correlations observed in the 2p radioactivity of  $^{94m}\text{Ag}$  have revealed strong proton yields either in the same or opposite directions which called for a theory of 2p emission from deformed nuclei [1]. Two-proton emission can also occur from short-lived nuclear resonances or excited states (see, e.g., [2, 3, 4]). Though in this case the mechanism of 2p emission may depend on the reaction populating the parent state, such nuclei can be easily studied in-flight. E.g., the cases of  $^6\text{Be}$  [2, 5] and  $^{16}\text{Ne}$  [6] were studied by analyzing their  $p-p$  correlations in the framework of a three-body partial-wave analysis developed for three-particle decays of light nuclei. In particular, the study of  $^6\text{Be}$  revealed the existence of three-particle  $p+p+\alpha$  correlations [2] which matched the three-body components found theoretically in the  $p$ -shell structure of  $^6\text{Be}$  [7]. Very recently,  $p-p$  correlations were also observed in 2p radioactivity of  $^{45}\text{Fe}$  [8, 9] where both the lifetime and  $p-p$  correlations were found to reflect the structure of  $pf$ -shell 2p precursors [9]. Such a way of obtaining spectroscopic information is a novel feature compared to studies of two-particle decays.

In the present paper, we study for the first time the  $p-p$  correlations in  $sd$  shell nuclei via examples of the 2p decays of  $^{19}\text{Mg}$  and  $^{16}\text{Ne}$ . These nuclei with very different half lives ( $T_{1/2} \approx 4 \cdot 10^{-9}$  s [10] and  $T_{1/2} \approx 4 \cdot 10^{-19}$  s [11], respectively) and presumably different spectroscopic properties may serve as reference cases illuminating the nuclear structure of other possible 2p emitters with  $sd$ -wave configuration.

The decay properties of the  $^{16}\text{Ne}$  and  $^{19}\text{Mg}$  ground states and the related resonances in  $^{15}\text{F}$  and  $^{18}\text{Na}$  are shown in Fig. 1 which compiles the data from Refs. [10, 11, 12, 13, 14, 15, 16] and this work. The ground states of both isotopes decay only by simultaneous 2p emission while their excited states are open for sequential 1p decays via intermediate unbound states in  $^{15}\text{F}$  and  $^{18}\text{Na}$ .

The quantum-mechanical theory of 2p radioactivity which uses a three-body model [17, 18, 19], predicts the  $p-p$  correlations to be strongly influenced by nuclear structure together with Coulomb and three-body centrifugal barriers. In particular, the newly discovered 2p-radioactivity of  $^{19}\text{Mg}$  [10] was predicted to be characterized by  $p-p$  correlations which reflect the  $sd$  configurations of the valence protons [20]. A similar effect is found in  $^{16}\text{Ne}$ , where the  $s$ -wave configuration was predicted to dominate, contrary to its mirror  $^{16}\text{C}$ , thus breaking isospin symmetry [21]. A complementary approach in describing 2p decays is the mechanism of sequential emission of protons via an intermediate state (see e.g., [22]). It includes also the traditional quasi-classical di-proton model with emission of a  $^2\text{He}$  cluster, assuming extremely strong  $p-p$  correlations [23, 24]. The predictions of these models differ dramatically with respect to the  $p-p$  correlations, suggesting them as a sensitive

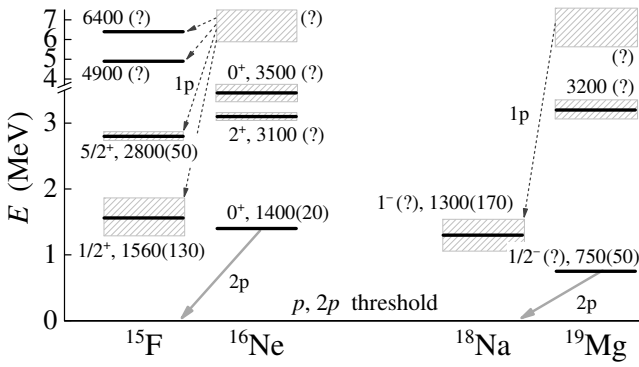


FIG. 1: States observed in  $^{16}\text{Ne}$ ,  $^{19}\text{Mg}$  and the corresponding intermediate systems  $^{15}\text{F}$ ,  $^{18}\text{Na}$ . Decay energies (in keV) are given relative to the respective p and 2p thresholds. Most values have been taken from the literature (Refs. [10, 11, 12, 13, 14, 15, 16]), those in bold print are from the present work.

probe of the 2p-decay mechanism (see the detailed predictions below).

Our experiment to investigate 2p-emission from  $^{19}\text{Mg}$  and  $^{16}\text{Ne}$  was performed by using a 591A MeV beam of  $^{24}\text{Mg}$  accelerated by the SIS facility at GSI, Darmstadt. The radioactive beams of  $^{20}\text{Mg}$  and  $^{17}\text{Ne}$  were produced at the Projectile-Fragment Separator (FRS) [25] with average intensities of 400 and 800 ions  $\text{s}^{-1}$  and energies of 450A and 410A MeV, respectively. The secondary 1-n-removal reactions ( $^{20}\text{Mg}$ ,  $^{19}\text{Mg}$ ) and ( $^{17}\text{Ne}$ ,  $^{16}\text{Ne}$ ) occurred at the mid-plane of FRS in a secondary 2 g/cm $^2$   $^9\text{Be}$  target. Special magnetic optics settings were applied, the first FRS half being tuned in an achromatic mode using a wedge-shaped degrader, while its second half was set for identification of the heavy ions (HI) with high acceptance in angle and momentum.

A sketch of the experimental set-up at the FRS mid-plane has been shown in Fig.1 of Ref. [10] and explained in detail there. A microstrip detector array [26] consisting of 4 large-area (7x4 cm $^2$ ) double-sided silicon detectors (with a pitch of 0.1 mm) was positioned downstream of the secondary target. This array was used to measure energy loss and position of coincident hits of two protons and a heavy fragment, thus allowing us to reconstruct all decay-product trajectories and derive the coordinates of the reaction vertex and the angular p-p and proton-HI correlations. The conditions to select the true HI+p+p events were: (i) a minimal distance between the proton and heavy ion trajectories of less than 150  $\mu\text{m}$ , and (ii) a difference between the two longitudinal coordinates of the vertices defined by two p-HI pairs (taken from the same HI+p+p event) within the range defined by the experimental uncertainty of 0.3–1 mm depending on detection angle. The achieved angular resolution in tracking the fragments was  $\sim 1$  mrad. More details concerning the detector performance and tracking procedure are given in [10, 27, 28, 29]. Another position-sensitive silicon detector and a multi-wire chamber were used upstream of

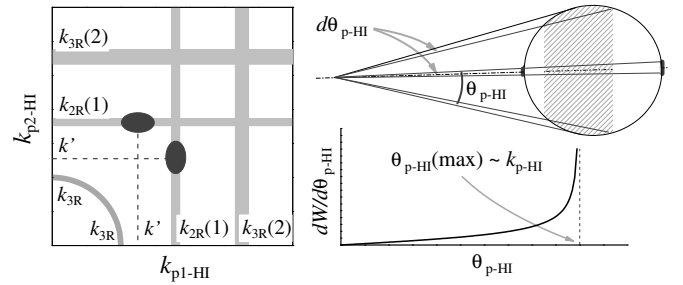


FIG. 2: Left panel: Cartoon of momentum correlations  $k_{p1-HI} - k_{p2-HI}$  expected for a direct three-body decay (the grey area labeled  $k_{3R}$ ) and sequential 2p decay (grey boxes with black peaks labeled  $k_{2R}$ ). Upper-right panel: A sketch of the kinematical enhancement of an angular p-HI correlation at the maximum possible angle for a given momentum between the decay products. Lower-right panel: the corresponding angular p-HI distribution.

the target for tracking the  $^{20}\text{Mg}$  ( $^{17}\text{Ne}$ ) projectiles. The heavy 2p-out residuals ( $^{17}\text{Ne}$  and  $^{14}\text{O}$ ) were unambiguously identified by their time of flight, magnetic rigidity, and energy loss measured with the position-sensitive scintillator detectors at the second half of FRS.

The 2p decays of the ground states of  $^{19}\text{Mg}$  and  $^{16}\text{Ne}$  were identified by using angular correlations between the single protons and their respective cores  $^{17}\text{Ne}$  and  $^{14}\text{O}$  which allowed measuring the 2p-decay energies. This is analogous to identifying a reaction via the scatter plot illustrated in Fig. 2 (left panel). In general, 2p-decay may proceed via either sequential or direct decay mechanisms. The first case can be described as two consecutive 1p decays, with the p-HI spectra reflecting the respective p-HI resonances [22]. Their (p $_1$ -HI)-(p $_2$ -HI) scatter plot should display the sequential and direct decay events in the respective kinematical areas marked in Fig. 2 by the relative momenta  $k_{2R}$ . In the second case, the simultaneously emitted protons are likely to share the 2p-decay energy evenly, with both p-HI spectra being identical and peaked at  $E/2$  [17, 24]. In this case, the area marked  $k_{3R}$  in Fig. 2 should be populated, along the arc area with the root-mean-squared proton momentum being constant. Sequential proton emission from a single 2p-parent state via narrow p-HI resonances should yield double peaks while 2p de-excitation of continuum parent states with p-HI final state interactions should reveal “slices” as shown in Fig. 2.

Similar structures can be found in the angular  $\theta_{p1-HI} - \theta_{p2-HI}$  correlations due to the following reason. Because of a strong kinematic focusing at intermediate energies, the 1p decay leads to a characteristic angular p-HI correlation when the proton ejected isotropically in the 1p-precursor frame is emitted within a narrow cone around the HI with the maximum intensity around the largest possible angle (Fig. 2, right panel). The p-HI angles reflect the transverse proton momentum relative to the HI one, and are therefore correlated with the precursor’s decay energy. Thus sequential 2p decays from ex-

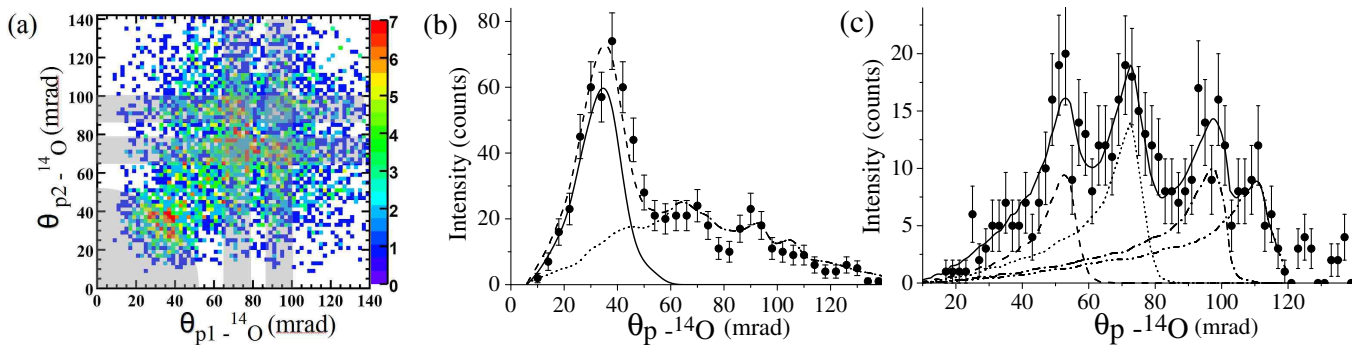


FIG. 3: (a) Angular  $(p_1-^{14}\text{O})-(p_2-^{14}\text{O})$  correlations obtained from the measured  $^{14}\text{O}+p+p$  events (colored boxes with scale shown on right). The grey areas indicate simultaneous and sequential 2p emission in analogy to those shown in Fig. 2. (b) Angular  $p-^{14}\text{O}$  distribution (full circles with statistical uncertainties) obtained from the data shown in panel (a) by selecting the other proton angle  $\theta_{p2-O}$  within the range from 0 to 45 mrad, which corresponds to the ground state of  $^{16}\text{Ne}$ . The solid curve represents the Monte Carlo simulation of the detector response for  $^{16}\text{Ne}_{g.s.} \rightarrow ^{14}\text{O}+p+p$  with a 2p-decay energy of 1.4(1) MeV [12]. The dashed line is a sum fit to the data. The dotted curve indicates the background as explained in the text. (c) Angular  $p-^{14}\text{O}$  distribution obtained from the data shown in (a) by selecting the other proton angle from 120 to 150 mrad, which corresponds to  $p-^{14}\text{O}$  final-state interactions due to the ground and excited states of  $^{15}\text{F}$ . The dashed and dotted curves are the Monte Carlo simulations of the known 1p decays of the ground and first excited states of  $^{15}\text{F}$  with the 1p-decay energies of 1.56(13) and 2.85(4) MeV, respectively [13]. The dash-dotted and dash-dot-dotted curves show the result of fits to the  $p-^{14}\text{O}$  correlation, indicating unknown excited states in  $^{15}\text{F}$  with 1p-decay energies of 4.9(2) and 6.4(2) MeV, respectively. The solid line is the sum fit.

cited states in parent nuclei should be mostly located in peaks with tails along the respective slices in the angular  $\theta_{p1-HI} - \theta_{p2-HI}$  correlations, in analogy to those sketched in Fig. 2 (left panel). In direct 2p decays, the single-proton energy spectrum always exhibits a relatively narrow peak centered close to half of the 2p-decay energy; such energy distribution is a stable feature of this decay mechanism [20, 23]. Correspondingly, a bump should appear in the angular correlations in the same way as it should appear along the arc marked by  $k_{3R}$  in the scatter plot in Fig. 2. This correspondence between angular and momentum correlations has been used to derive the 2p-decay energy of  $^{19}\text{Mg}$  (see Fig. 2,4 in [10] and the respective discussions).

For the 2p-decay of  $^{16}\text{Ne}$ , the angular correlations of each coincident proton with respect to the  $^{14}\text{O}$  momentum,  $\theta_{p1-O} - \theta_{p2-O}$ , derived from the measured  $^{14}\text{O}+p+p$  coincidence events, are shown in Fig. 3(a). The events with the smallest angles fall into a distinct cluster around  $\theta_{p-O}=35$  mrad while most of the other events are located in the slices centered around 70 and 95 mrad. These two groups can be attributed to the direct 2p decay from the  $^{16}\text{Ne}$  ground state and to the sequential emission of protons from excited states in  $^{16}\text{Ne}$  via the  $^{15}\text{F}$  ground-state, respectively. We shall refer to these events as the “ground state” and “excited state” events, respectively. The latter group includes also events resulting from the fragmentation reaction  $^{17}\text{Ne} \rightarrow ^{14}\text{O}+p+p+n$ .

To disentangle the “ground state” from the “excited state” events, we made a slice projection from the measured  $(p_1-^{14}\text{O})-(p_2-^{14}\text{O})$  correlations in Fig. 3(a) by selecting the angle of one of the protons within the range 0–45 mrad, where the 2p decay of the  $^{16}\text{Ne}$  ground state

is expected to show up. Figure 3(b) displays the angular correlations  $\theta_{p1-O}$  corresponding to the “ground state” gate in the other pair  $\theta_{p2-O}$ . The peak around 35 mrad (the suggested “ground state”) dominates the spectrum, whereas few correlations can be seen between a proton from the “ground state” and another proton at larger angles. This means that the two protons from the “ground-state” are correlated, i.e. this peak can be explained by an emission of protons from the ground state in  $^{16}\text{Ne}$ .

For a more quantitative analysis, the data are compared to a Monte Carlo simulation of the response of our setup to the direct 2p-decay  $^{16}\text{Ne} \rightarrow ^{14}\text{O}+p+p$  with the known 2p-decay energy of 1.4(1) MeV [12] by using the GEANT program [30]. The simulations took into account the above-mentioned experimental accuracies in tracking the fragments and in reconstructing the vertices, trajectory angles etc. The normalized simulation reproduces the data in the low-angle peak very well. The contribution from the “tail” of the higher states to the ground-state peak amounts to about 20%. The shape of this distribution is assumed to have the same shape as the  $\theta_{p1-O}$  distribution selected within the  $\theta_{p2-O}$  range just outside the ground-state region, from 48 to 160 mrad (the dotted curve).

Figure 3(c) displays an example of an angular  $p-^{14}\text{O}$  distribution for “excited states” obtained from Fig. 3(a) by selecting the angular range of the other proton from 120 to 150 mrad, which corresponds to  $p-^{14}\text{O}$  final state interactions due to the ground and excited states of  $^{15}\text{F}$ . The Monte Carlo simulation of known one-proton decays  $^{15}\text{F} \rightarrow ^{14}\text{O}+p$  of the ground and first excited states in  $^{15}\text{F}$  with the 1p-decay energies of 1.56(13) and 2.85(4) MeV [13], respectively, reproduces well the two lowest-angle

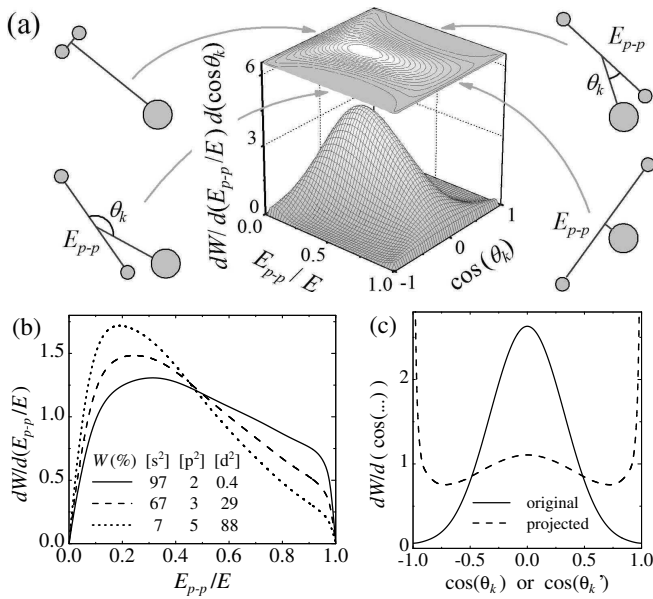


FIG. 4: (a) Three-body correlations predicted by the three-body model [20] for the 2p-decay of  $^{19}\text{Mg}$ , plotted as a function of the relative energy between two protons,  $E_{p-p}/E$ , and the angle  $\theta_k$  between the relative momenta of the fragments as illustrated in the figure. Extreme cases of p-p correlations are sketched and related to the corresponding areas in the correlation plot. (b) The p-p energy spectra from the 2p-decay of  $^{19}\text{Mg}$  calculated for different weights  $W$  of  $s$ - $p$ - $d$  shell configurations in  $^{19}\text{Mg}$ . (c) Typical intensity distributions plotted as a function of  $\theta_k$  (see Fig. 4(a)) in the rest frame of the 2p-precursor (solid curve) and its analog in the lab system  $\theta'_k$  projected on the transverse detector plane (dashed curve).

peaks. The two higher-lying peaks indicate 1p decays of unknown excited states in  $^{15}\text{F}$  with derived 1p-decay energies of 4.9(2) and 6.4(2) MeV. The excited states in  $^{19}\text{Mg}$ ,  $^{16}\text{Ne}$ ,  $^{18}\text{Na}$  and  $^{15}\text{F}$  will be addressed elsewhere.

We turn now to the discussion of angular p-p correlations following 2p decays. When the spin degrees of freedom are neglected and the total decay energy  $E$  can be considered as fixed, the three-body correlations are completely described by two variables. A convenient choice is an energy-distribution parameter  $E_{p-p}/E$  ( $E_{p-p}$  is relative energy between two protons) and an angle  $\theta_k$  between the relative momenta of the fragments. Fig. 4 shows such distributions predicted by the three-body model for the 2p-decay of  $^{19}\text{Mg}$  [19, 20]. The three-body model predicts a distinctive correlation pattern which features an enhancement at small  $E_{p-p}$  due to final-state interaction and a suppression in the regions of strong Coulomb repulsion ( $E_{p-p}/E \sim 0.5$ ,  $\cos(\theta_k) \sim \pm 1$ ). The predicted energy distributions are sensitive to the structure of the precursor [Fig. 4(b)]. Similar predictions are available for  $^{16}\text{Ne}$  [21].

In our experiment, we were able to measure the opening angle  $\theta_{p-p}$  between protons whose distribution reflects the  $E_{p-p}$  correlations. Fig. 5 shows the experimental angular p-p distributions obtained from triple

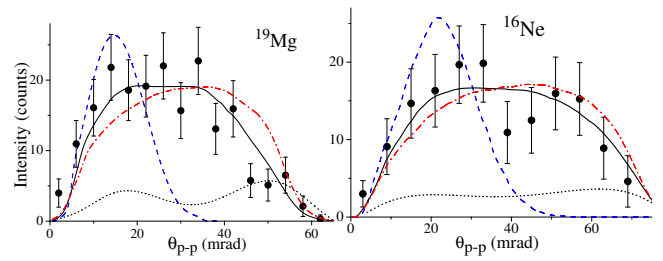


FIG. 5: Angular p-p correlations from the 2p-decays of the ground states of  $^{19}\text{Mg}$  (left) and  $^{16}\text{Ne}$  (right) obtained from the measured  $^{14}\text{O}+p+p$  and  $^{17}\text{Ne}+p+p$  events, respectively, by selecting both protons from the respective  $p-^{14}\text{O}$  ( $^{17}\text{Ne}$ ) angular ranges. The solid curves show the fits to the data, obtained by using the three-body model calculations (54% and 88% of  $d$ -wave configuration in  $^{16}\text{Ne}$  and  $^{19}\text{Mg}$ , respectively). The dotted curves show the background contributions estimated as described in the text. The dashed curves are the dipron model predictions, and the dash-dotted curves are the phase-space simulations of the 2p-decays (isotropic proton emission in the 2p-precursor's rest frame).

$^{14}\text{O}+p+p$  and  $^{17}\text{Ne}+p+p$  events gated by the conditions that both protons originate from the “ground states” of  $^{16}\text{Ne}$  and  $^{19}\text{Mg}$ . These gates were inferred from the respective angular p-HI correlations as discussed above. The events representing the “ground state” 2p decay actually contain contributions from the ground state and background contributions from both, excited states of the parent nucleus and fragmentation reactions. Therefore, using the angular-correlation data discussed above, we empirically evaluated the shapes of the background components by projecting triple events with the p-HI gates shifted away from the “ground state” region towards larger angles. The resulting p-p background contributions shown by the dotted curves in Fig. 5 constitute about 20 % of all p-p correlation data for  $^{16}\text{Ne}$  and 25 % for  $^{19}\text{Mg}$  (see Fig. 3(b) and Fig. 4 (c) in [10]); they were subtracted from the original p-p correlations. As one can see in Fig. 5, the predictions following from the assumption of a diproton emission fail to describe both the  $^{16}\text{Ne}$  and  $^{19}\text{Mg}$  data while the three-body model reproduces the shapes of both distributions. In the  $^{19}\text{Mg}$  case, the best description is obtained with the  $d$ -wave configuration dominating. The  $^{16}\text{Ne}$  data give evidence for nearly equal  $s$ - and  $d$ -wave components.

In Fig. 6, the intensity distributions are displayed as a function of  $\cos(\theta'_k)$ . The angle  $\theta'_k$  (see Fig. 4(a)) was defined by a line connecting the two points where two protons hit the same detector and by a vector joining the middle between the 2p hits and the point of a related heavy-ion hit, in analogy with the angle  $\theta_k$  shown in Fig. 4(a). The typical theoretical prediction for such a distribution is shown in Fig. 4(c). The diproton model predicts flat angular distributions in contrast to the experimental data in both cases. Only the three-body model can reproduce the characteristic shapes of the observed correlations with the broad bumps around

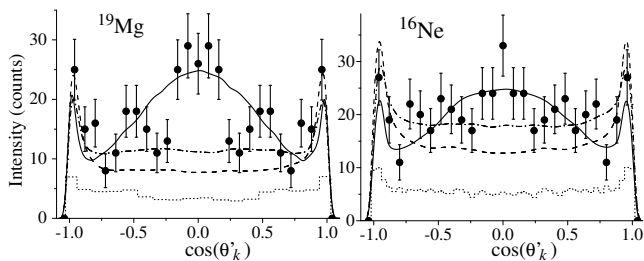


FIG. 6: Three-body correlations from the 2p-decays of the ground states of  $^{16}\text{Ne}$  and  $^{19}\text{Mg}$  (full circles with statistical uncertainties) obtained from the measured  $^{14}\text{O}+p+p$  and  $^{17}\text{Ne}+p+p$  events by selecting an angle  $\theta'_k$  (see text). The solid curves are the three-body model calculations (assuming 54% and 88% of  $d$ -wave configuration in  $^{16}\text{Ne}$  and  $^{19}\text{Mg}$ , respectively). The dashed curves are the diproton model predictions, and the dash-dotted curves are the phase-space simulations illustrating the response to an isotropic 2p-emission in the precursor's rest frames (both simulations are not normalized). The dotted curves show the background contributions estimated from all measured  $\text{HI}+p+p$  events.

$\cos(\theta'_k)=0$  (the indicated spikes at  $\cos(\theta'_k)\approx\pm 1$  predicted by all calculations are less conclusive). Such a shape is a manifestation of the “Coulomb focusing” efficiently repulsing the fragments from large regions of the momentum space (see Fig. 4(a)). These distributions are weakly sensitive to the assumed structure of the parent states but are an exclusive feature of the three-body model.

In summary, the measured three-particle correlations from the 2p decay of the ground states of  $^{16}\text{Ne}$  and  $^{19}\text{Mg}$

are described quantitatively by the predictions of the tree-body model [20], in contrast to the quasi-classical “diproton” model which fails to describe our observations. These correlations are sensitive to the structure of the decaying nucleus. Thus the comparison between experiment and theory allows one to obtain spectroscopic information about the parent states. In  $^{16}\text{Ne}$ , the data are consistent with strong  $s/d$  mixing [21]. In  $^{19}\text{Mg}$ , the dominating  $d$ -shell configuration is the preferable description which is also consistent with the lifetime information [10]. The method of measuring 2p-decays in flight by precisely tracking all fragments with microstrip detectors provides new specific observables, thus yielding valuable spectroscopic information on such exotic isotopes. Information about two-body subsystems, e.g.,  $^{15}\text{F}$ , is simultaneously obtained. Systematic studies of other 2p emitters predicted theoretically [19, 31] are foreseen with this novel technique.

The authors are grateful to M. Pohl and his co-workers of the DPNC, Université de Genève, for developing the microstrip detectors. We thank in particular E. Cortina for the valuable contribution to this project. We appreciate the help of A. Bruenle, K.H. Behr, W. Hueller, A. Kelic, A. Kiseleva, R. Raabe and O. Tarasov during the preparations of the experiment. This work has been supported by contracts EURONS No. EC-I3 and FPA2003-05958, FPA2006-13807-C02-01 (MEC, Spain), the INTAS grant 03-54-6545, the Russian RFBR grants 05-02-16404 and 05-02-17535 and the Russian Ministry of Industry and Science grant NS-1885.2003.2.

- 
- [1] I. Mukha *et al.*, *Nature*(London) **439**, 298 (2006).
  - [2] O.V. Bochkarev *et al.*, *Nucl. Phys.* **A505**, 215 (1989).
  - [3] R.A. Kryger *et al.*, *Phys. Rev. Lett.* **74**, 860 (1995).
  - [4] C.R. Bain *et al.*, *Phys. Lett. B* **373**, 35 (1996).
  - [5] B.V. Danilin *et al.*, *Sov. J. Nucl. Phys.* **46**, 225 (1987).
  - [6] A.A. Korshennikov, *Sov. J. Nucl. Phys.* **52**, 827 (1990).
  - [7] I.J. Thompson *et al.*, *Phys. Rev. C* **61**, 024318 (2000).
  - [8] J. Giovinazzo *et al.*, *Phys. Rev. Lett.* **99**, 102501 (2007).
  - [9] K. Miernik *et al.*, *Phys. Rev. Lett.* **99**, 192501 (2007).
  - [10] I. Mukha *et al.*, *Phys. Rev. Lett.* **99**, 182501 (2007).
  - [11] G.J. KeKelis *et al.*, *Phys. Rev. C* **17**, 1929 (1978).
  - [12] C.J. Woodward, R.E. Tribble and D.M. Tanner, *Phys. Rev. C* **27**, 27 (1983).
  - [13] A. Lepine-Szily *et al.*, *Nucl. Phys.* **A734**, 331 (2004).
  - [14] W.A. Peters *et al.*, *Phys. Rev. C* **68**, 034607 (2003).
  - [15] V.Z. Goldberg *et al.*, *Phys. Rev. C* **69**, 031302(R) (2004).
  - [16] T. Zerguerras *et al.*, *Eur. Phys. J. A* **20**, 389 (2004).
  - [17] L.V. Grigorenko, R.C. Johnson, I.G. Mukha, I.J. Thompson, and M.V. Zhukov, *Phys. Rev. Lett.* **85**, 22 (2000).
  - [18] L.V. Grigorenko, R.C. Johnson, I.G. Mukha, I.J. Thompson, and M.V. Zhukov, *Phys. Rev. C* **64**, 054002 (2001).
  - [19] L.V. Grigorenko and M.V. Zhukov, *Phys. Rev. C* **68**, 054005 (2003).
  - [20] L.V. Grigorenko, I.G. Mukha, and M.V. Zhukov, *Nucl. Phys.* **A713**, 372 (2003); **A740**, 401(E) (2004).
  - [21] L.V. Grigorenko, I.G. Mukha, I.J. Thompson, and M.V. Zhukov, *Phys. Rev. Lett.* **88**, 042502 (2002).
  - [22] A.M. Lane and R.G. Thomas, *Rev. of Mod. Phys.* **30**, 257 (1958).
  - [23] V.I. Goldansky, *Nucl. Phys.* **19**, 482 (1960).
  - [24] A.I. Baz', V.I. Goldansky, V.Z. Goldberg and Ya.B. Zel'dovich, *Light and Intermediate Nuclei Near the Border of Nuclear Stability* (Nauka, Moscow, 1972).
  - [25] H. Geissel *et al.*, *Nucl. Instrum. Methods Phys. Res. B* **70**, 286 (1992).
  - [26] <http://dpnc.unige.ch/ams/GSItracker/www/>.
  - [27] M. Stanoiu *et al.*, GSI Scientific Report 2006, p. 23.
  - [28] I. Mukha *et al.*, GSI Scientific Report 2006, p. 112.
  - [29] J. Hoffmann, N. Kurz and W. Ott, GSI Scientific Report 2006, p. 216.
  - [30] “GEANT - detector simulation tool”, CERN software library, <http://wwwasd.web.cern.ch/wwwasd/geant>.
  - [31] L.V. Grigorenko, I.G. Mukha and M.V. Zhukov, *Nucl. Phys.* **A714**, 425 (2003).